


## Polarization conversion metasurface in terahertz region

Chen Zhou(周晨), Jiu-Sheng Li(李九生)

**Citation:**Chin. Phys. B . 2020, 29(7): 078706 . **doi:** 10.1088/1674-1056/ab9295
Journal homepage: http://cpb.iphy.ac.cn; http://iopscience.iop.org/cpb

**What follows is a list of articles you may be interested in**

---

## Terahertz polarization conversion and sensing with double-layer chiral metasurface

Zi-Yang Zhang(张子扬), Fei Fan(范飞), Teng-Fei Li(李腾飞), Yun-Yun Ji(冀允允), Sheng-Jiang Chang(常胜江)
Chin. Phys. B . 2020, 29(7): 078707 . **doi:** 10.1088/1674-1056/ab9294

## Effect of terahertz pulse on gene expression in human eye cells

Jin-Wu Zhao(赵晋武), Ming-Xia He(何明霞), Li-Jie Dong(东莉洁), Shao-Xian Li(李绍限), Li-Yuan Liu(刘立媛), Shao-Chong Bu(步绍翀), Chun-Mei Ouyang(欧阳春梅), Peng-Fei Wang(王鹏驰), Long-Ling Sun(孙珑玲)
Chin. Phys. B . 2019, 28(4): 048703 . **doi:** 10.1088/1674-1056/28/4/048703

## Ultra-compact terahertz switch with graphene ring resonators

Jian-Zhong Sun(孙建忠), Le Zhang(章乐), Fei Gao(高飞)
Chin. Phys. B . 2016, 25(10): 108701 . **doi:** 10.1088/1674-1056/25/10/108701

## Design and optimization of terahertz directional coupler based on hybrid-cladding hollow waveguide with low confinement loss

Yu Ying-Ying, Li Xu-You, Sun Bo, He Kun-Peng
Chin. Phys. B . 2015, 24(6): 068702 . **doi:** 10.1088/1674-1056/24/6/068702

## Realization of a broadband terahertz wavelength-selective coupling based on five-core fibers

Li Xu-You, Yu Ying-Ying, Sun Bo, He Kun-Peng
Chin. Phys. B . 2014, 23(8): 088701 . **doi:** 10.1088/1674-1056/23/8/088701

---

SPECIAL TOPIC — Terahertz physics

# Polarization conversion metasurface in terahertz region*

Chen Zhou(周晨)[1] and Jiu-Sheng Li(李九生)[1,2,†]

[1] Centre for THz Research, China Jiliang University, Hangzhou 310018, China
[2] China Key Laboratory of Electromagnetic Wave Information Technology and Metrology of Zhejiang Province, College of Information Engineering, China Jiliang University, Hangzhou 310018, China

(Received 29 March 2020; revised manuscript received 24 April 2020; accepted manuscript online 13 May 2020)

Polarization conversion is a very important electromagnetic wave manipulation method. In this paper, we investigate a high-efficiency linear-to-circular polarization and cross-polarization converter by utilizing coding metasurface. The coding particle consists of top layer metal pattern and bottom metal plate sandwiched with square F4B dielectric, which can manipulate the linear-to-circular polarization and cross-polarization converter of the reflected wave simultaneously. In the terahertz frequency range of 1.0 THz–2.0 THz, the reflection magnitudes reach approximately 90% and the axial ratio is less than 3 dB. The proposed polarization converter may lead to advances in a variety of applications such as security, microscopy, information processing, stealth technology, and data storage.

**Keywords:** terahertz wave, polarization conversion, metasurface

**PACS:** 87.50.–a, 87.50.up, 87.10.Vg **DOI:** 10.1088/1674-1056/ab9295

## 1. Introduction

The metasurface consists of sub-wavelength unit structures of different phases, due to its thin thickness and low loss, it has a strong manipulation ability in terms of phase, polarization, and amplitude of electromagnetic waves.[1–3] Therefore, it has been widely used in the regulation of electromagnetic wave such as electromagnetic stealth technology,[4,5] anomalous reflection and refraction,[6] polarization conversion,[8–10] and holographic technology.[11] For the last few years, the coding metasurface based on binary digital codes "0" and "1" have been proposed. More recently, anisotropic coding metasurfaces have been proposed which have different responses to two orthogonally polarized electromagnetic waves.[12,13] When the metasurface is designed as a binary digital pattern, the different predesigned coding sequences can achieve the anomalous reflection and diffusion scattering of electromagnetic waves.[14–16] These reported coding metasurfaces provide a new scheme for manipulating the transmitted and reflected electromagnetic waves by altering their phase and amplitude at will.[17] To our best knowledge, polarization state change is also a way to control electromagnetic waves. Although great progress has been made in the research of coding metasurfaces, there is little research on polarization conversion using coding metasurfaces.

In this paper, we designe and investigate a novel coding metasurface based on cross-polarization phase gradient to realize polarization conversion in terahertz region. The coding particle of the proposed coding metasurface consists of top layer metal pattern and bottom metal plate sandwiched with square F4B dielectric, which can manipulate the linear-to-circular polarization conversion and cross polarization conversion of the normal incidence terahertz wave simultaneously. This coding metasurface can achieve complete reflection phase coverage from 0 to $2\pi$ at frequency range from 1.0 THz to 2.0 THz, where the axial ratio is less than 3 dB. Our finding significantly improves efficiency of polarization conversion and offers a new approach for terahertz manipulation.

## 2. Coding particle design

Figures 1(a) and 1(b) show the perspective view schematic diagrams of the proposed coding particle structures and four types of coding particles for coding metasurfaces. The coding particles are composed of three layers with the period of $P = 70$ μm. The intermediate layer is an F4B dielectric ($\varepsilon_r = 2.65$, $\tan\delta = 0.001$) with a thickness of $h = 30$ μm. The bottom metal plate and the top metal patterns are made of copper ($\varepsilon_r = 5.8 \times 10^7$ S/m) with a thickness of 0.2 μm. The optimized geometrical parameters of the metasurface pattern are as follows: $a = 66$ μm, $b = 20$ μm, $w_1 = 5$ μm, $w_2 = 2$ μm, $w_3 = 3.5$ μm, $r = 34$ μm, $c = 41$ μm, $g = 19$ μm, $L = 5.5$ μm, $\gamma = 100°$, and $d = 14$ μm. In Fig. 1(b), we design four types of coding particles, which can independently reflect the normal incidence with reflection phase of 0° or 180° under left circularly polarized plane (LCP) or right circularly polarized plane (RCP). Here, "00" and "11" or "01" and "10" digital codes have the same coding particle structures by rotated 90° of the top layer metal pattern.

*Project supported by the National Key Research and Development Program of China (Grant No. 2016YFF0200306) and the National Natural Science Foundation of China (Grant Nos. 61871355 and 61831012).

†Corresponding author. E-mail: jshli@126.com

© 2020 Chinese Physical Society and IOP Publishing Ltd 

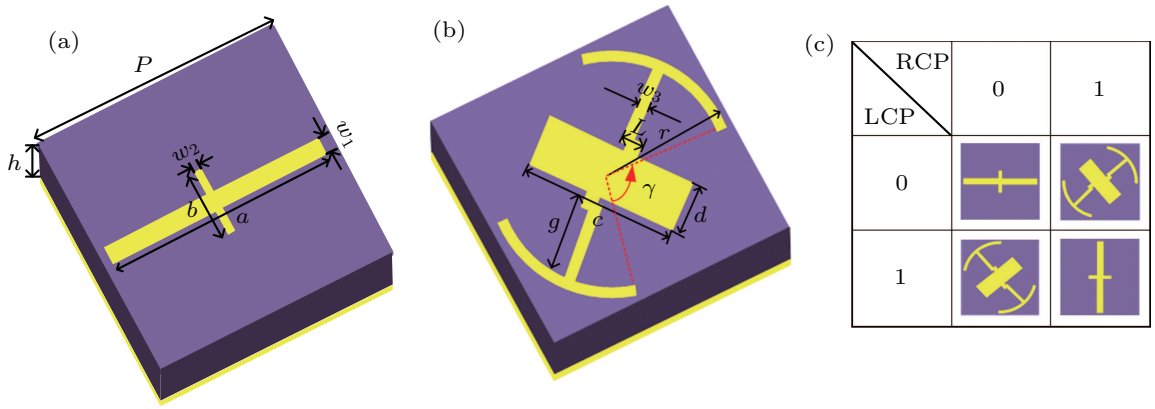



**Fig. 1.** (a) and (b) Perspective view schematic diagrams of the proposed coding particle, (c) four kinds of coding particles.

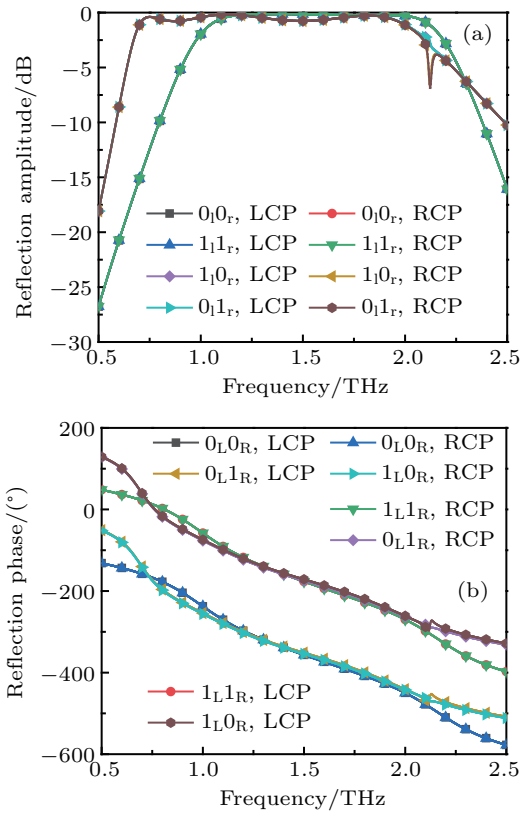



**Fig. 2.** (a) Cross-polarized reflection amplitudes, (b) reflection phase at normal incidence of LCP and RCP.

By using the software CST Microwave Studio, we get the cross-polarized reflection and reflection phases of the coding particles in the frequency from 0.5 THz to 2.5 THz for LCP and RCP waves incidences, as shown in Figs. 2(a) and 2(b). From Fig. 2(a), one can see that the cross-polarized reflection amplitudes of the coding particles are less than $-1$ dB. Under the circularly polarized waves LCP normal incidence, the LCP wave converts to RCP wave, and *vice versa*. In order to analyze the polarization conversion performance of the coding particles, we define the polarization conversion efficiency $R_{\mathrm{PC}} = R_{ij}^2/(R_{ij}^2 + R_{ii}^2)$, where $R_{ii}$ and $R_{ij}$ represent the co-polarized and cross-polarized reflection coefficient, respectively. In Fig. 2(a), when the cross-polarization reflection amplitude approaches 1, the co-polarization reflection amplitude tends to 0. According to the polarization conversion formula, it is easy to get the polarization conversion ratio close to 1 in the frequency ranging from 1.0 THz to 2.0 THz. From Fig. 2(b), we can observe that the cross-polarized reflection phase with a phase difference close to close to $\pi$ between "0" and "1" coding particles. We have designed "$0_{\mathrm{L}}0_{\mathrm{R}}$", "$1_{\mathrm{L}}1_{\mathrm{R}}$", "$0_{\mathrm{L}}1_{\mathrm{R}}$", and "$1_{\mathrm{L}}0_{\mathrm{R}}$" four types of coding particles corresponding to digital codes "0" or "1" under normal incidence of LCP or RCP. Here, the subscript "L" and "R" denote LCP and RCP waves, respectively.

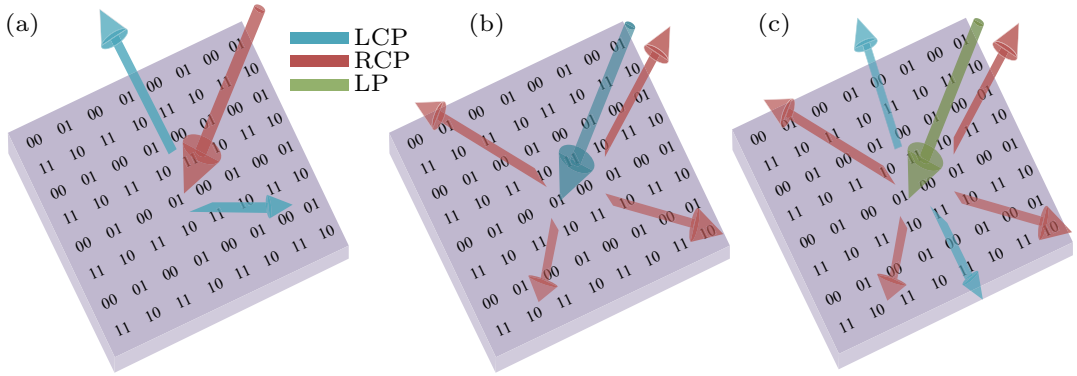



**Fig. 3.** Schematic diagrams of different polarized waves illuminate coding metasurface: (a) normal incidence RCP wave converts to the reflected two LCP wave beams. (b) Normal incidence LCP wave converts to the reflected four RCP wave beams, (c) LP wave normal incidence converts to the reflected two LCP wave beams and four RCP wave beams.

To illustrate the ability of coding metasurface to transform linearly polarized (LP) wave into circularly polarized (CP) wave, we design a new coding metasurface to verify this principle. According to the basic theory of electromagnetic field, the CP wave can be decomposed into two LP waves which are orthogonal to each other, with equal amplitude and phase difference of 90°. Therefore, when the anisotropic coding metasurface is irradiated by LP wave, the linear-to-circularly polarization conversion can be realized and the beam deflection can be realized at the same time. The predesigned coding sequence consists of four basic coding particles [$0_L0_R$, $0_L1_R$, $1_L0_R$, $1_L1_R$]. As shown in Fig. 3(a), under normal incidence of RCP, the coding sequence of the coding metasurface likes [0,0; 1,1] and the incidence terahertz wave is divided into two equal LCP waves. As depicted in Fig. 3(b), in the case of normal incidence of LCP, predesigned coding sequence of the coding metasurface becomes [0,1; 1,0] and the incidence terahertz wave is divided into four symmetrical RCP waves. When the coding metasurface is illuminated by using LP wave, it is converted into CP wave, as depicted in Fig. 3(c).

In this case, the reflection coefficient matrix of linear polarization can be expressed as

$$\begin{pmatrix} r_{xx} & r_{xy} \\ r_{yx} & r_{yy} \end{pmatrix} = \begin{pmatrix} \cos\alpha + \mathrm{j}\sin\alpha & 0 \\ 0 & \cos(\alpha-\pi) + \mathrm{j}\sin(\alpha-\pi) \end{pmatrix}, \quad (1)$$

where $\alpha$ is the reflection phase of the $x$-polarized incidence, $(\alpha-\pi)$ is the reflection phase of the $y$-polarized incidence, and the subscripts $x$ and $y$ denote the polarization of incidence terahertz wave. The reflection coefficient matrix for circular polarization is related to the matrix linear Jones matrix. The reflection coefficient of circular polarization can be calculated by

$$\begin{aligned} r_{\mathrm{LL}} &= \frac{1}{2}[(r_{xx}-r_{yy}) - \mathrm{j}(r_{xy}+r_{yx})]\,\mathrm{e}^{-\mathrm{j}2\theta}, \\ r_{\mathrm{RR}} &= \frac{1}{2}[(r_{xx}-r_{yy}) + \mathrm{j}(r_{xy}+r_{yx})]\,\mathrm{e}^{\mathrm{j}2\theta}, \\ r_{\mathrm{LR}} &= \frac{1}{2}[(r_{xx}+r_{yy}) + \mathrm{j}(r_{xy}-r_{yx})], \\ r_{\mathrm{LR}} &= \frac{1}{2}[(r_{xx}+r_{yy}) - \mathrm{j}(r_{xy}-r_{yx})], \end{aligned} \quad (2)$$

where $\theta$ is the rotation angle of the coding particle. Figure 4(a) shows the reflection amplitude of the unrotated coding particles under the incidence of linear polarization wave.

It can be observed that $r_{xx}$ and $r_{yy}$ are close to 1, and $r_{yx}$ and $r_{xy}$ are close to 0. Then, the reflection coefficient matrix of the circular polarization wave incidence can be given by

$$\begin{pmatrix} r_{\mathrm{LL}} & r_{\mathrm{LR}} \\ r_{\mathrm{RL}} & r_{\mathrm{RR}} \end{pmatrix} = \begin{pmatrix} 0 & 1 \\ 1 & 0 \end{pmatrix}. \quad (3)$$

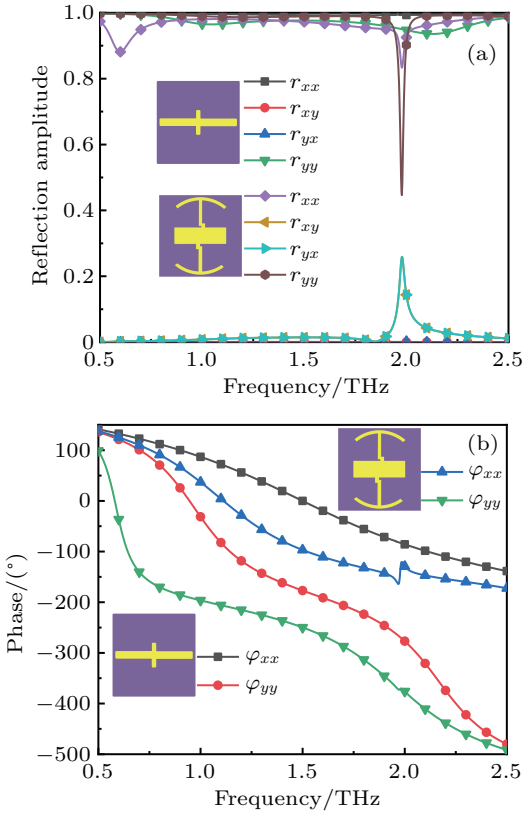
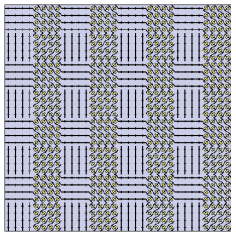



**Fig. 4.** (a) Reflection amplitude, (b) co-polarized reflection phase of the coding particle under LP polarization incidence.

Figure 4(b) shows the reflection phase for $x$-polarized and $y$-polarized incidences. There is a phase difference of $\pi$ between the reflection phase of the basic coding particle under $x$-polarized and $y$-polarized incidences.

For the quantitative description of the coding metasurfaces, we designed a kind of coding metasurface with coding matrix $S_1$ and the predesigned coding sequence of "$0_L0_R$, $0_L1_R$, $0_L0_R$, $0_L1_R$, $0_L0_R$, $0_L1_R$, $0_L0_R$, $0_L1_R/1_L0_R$, $1_L1_R$, $1_L0_R$, $1_L1_R$, $1_L0_R$, $1_L1_R$, $1_L0_R$, $1_L1_R$..." as shown in the following figure (Fig. 5).

$$S_1 = \begin{bmatrix} 0_L0_R & 0_L1_R & 0_L0_R & 0_L1_R & 0_L0_R & 0_L1_R & 0_L0_R & 0_L1_R \\ 1_L1_R & 1_L0_R & 1_L1_R & 1_L0_R & 1_L1_R & 1_L0_R & 1_L1_R & 1_L0_R \\ 0_L0_R & 0_L1_R & 0_L0_R & 0_L1_R & 0_L0_R & 0_L1_R & 0_L0_R & 0_L1_R \\ 1_L1_R & 1_L0_R & 1_L1_R & 1_L0_R & 1_L1_R & 1_L0_R & 1_L1_R & 1_L0_R \\ 0_L0_R & 0_L1_R & 0_L0_R & 0_L1_R & 0_L0_R & 0_L1_R & 0_L0_R & 0_L1_R \\ 1_L1_R & 1_L0_R & 1_L1_R & 1_L0_R & 1_L1_R & 1_L0_R & 1_L1_R & 1_L0_R \\ 0_L0_R & 0_L1_R & 0_L0_R & 0_L1_R & 0_L0_R & 0_L1_R & 0_L0_R & 0_L1_R \\ 1_L1_R & 1_L0_R & 1_L1_R & 1_L0_R & 1_L1_R & 1_L0_R & 1_L1_R & 1_L0_R \end{bmatrix}$$



(a) (b)

**Fig. 5.** Coding matrix of $S_1$ (a) and schematic diagram (b) of coding metasurface based on $S_1$.

In order to minimize the coupling effects between different particle types, each type is grouped into $4\times4$ sub-arrays of identical particles and then assembled into $2\times2$ arrays of the four particle types so that the fill surface looks like that as shown in Fig. 5(b).

## 3. Results and discussion

To demonstrate the previous analysis as above, we calculated three-dimensional (3D) and two-dimensional (2D) far-field scattering pattern of the coding metasurface under the normal incidence of the RCP, LCP, and LP waves at 1.85 THz, respectively. Figures 6(a) and 6(c) show 3D and 2D far-field scattering patterns of the coding metasurface under the normal incidence of RCP wave. At this time, the two symmetrically reflected LCP waves have the angle of $(\theta_1, \varphi_1) = (16.83°, 90°)$ and $(\theta_1, \varphi_2) = (16.83°, 270°)$. Similarly, as illustrated in Figs. 6(b) and 6(d), under the normal incidence of LCP wave, four symmetrically reflected RCP waves with their reflection angles of $(\theta_2, \varphi_1) = (24.17°, 45°)$, $(\theta_2, \varphi_2) = (24.17°, 135°)$, $(\theta_2, \varphi_3) = (24.17°, 225°)$, and $(\theta_2, \varphi_4) = (24.17°, 315°)$, respectively. Because the designed coding units all have cross polarization conversion characteristics, when the coding metasurface under the incidence of the CP wave can achieve cross-polarization conversion in circular polarization greatly.

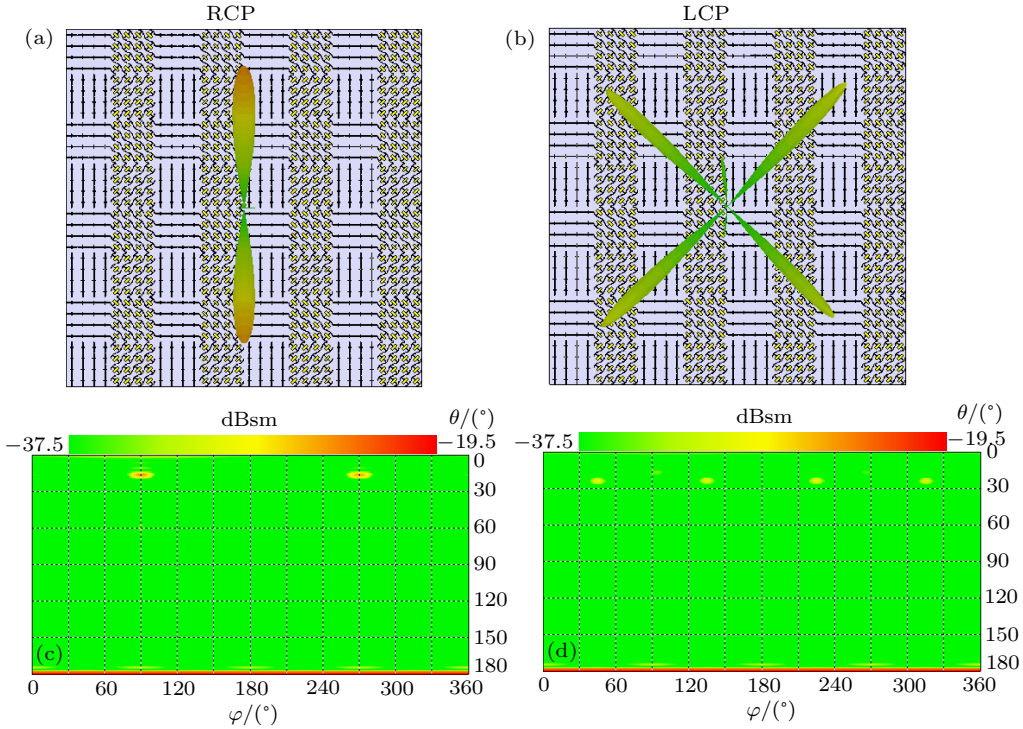



**Fig. 6.** 3D and 2D far-field scattering patterns of the $S_1$ coding metasurface under normal incidence at 1.85 THz for RCP incidence [(a) and (c)] and that for LCP incidence [(b) and (d)].

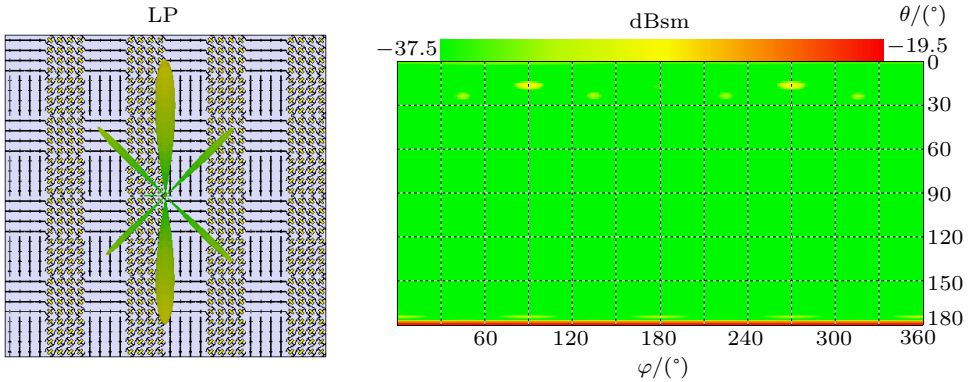



**Fig. 7.** 3D and 2D far-field scattering patterns of the $S_1$ coding metasurface under normal incidence of LP wave at 1.85 THz.

As depicted in Figs. 7(a) and 7(b), the normal incidence LP wave transforms into two symmetrically reflected LCP waves and four symmetrically reflected RCP waves. The condition to realize the linear-to-circular polarization conversion is that the incidence of LP wave is decomposed into two mutually orthogonal LP waves with the same amplitude and phase difference of 90°. As shown in Fig. 4, the designed coding unit meets such a standard. Their azimuth angles are $(\theta_1, \varphi_1) = (16.83°, 90°)$, $(\theta_1, \varphi_2) = (16.83°, 270°)$, $(\theta_2, \varphi_3) = (24.17°, 45°)$, $(\theta_2, \varphi_4) = (24.17°, 135°)$, $(\theta_2, \varphi_5) = (24.17°, 225°)$, and $(\theta_2, \varphi_6) = (24.17°, 315°)$, respectively. The polarization conversion characteristics can be elaborated

upon the axial ratio and scattering pattern at three azimuth angles $\varphi = 90°$, 45°, and 225°, as shown in Fig. 8. When $\varphi = 90°$ (see Fig. 8(a)), the axial ratio approaches 3 dB at $\theta = \pm 16.83°$, and the normal incidence of LP wave can be converted into CP wave as we expected. Figures 8(b) and 8(c) depict the axial ratio and scattering pattern of the presented coding metasurface at $\varphi = 45°$ and $\varphi = 225°$. One can see that the axial ratio is less than 3 dB at $\theta = 24.17°$. Thus, LP wave can be transformed into CP wave efficiently.

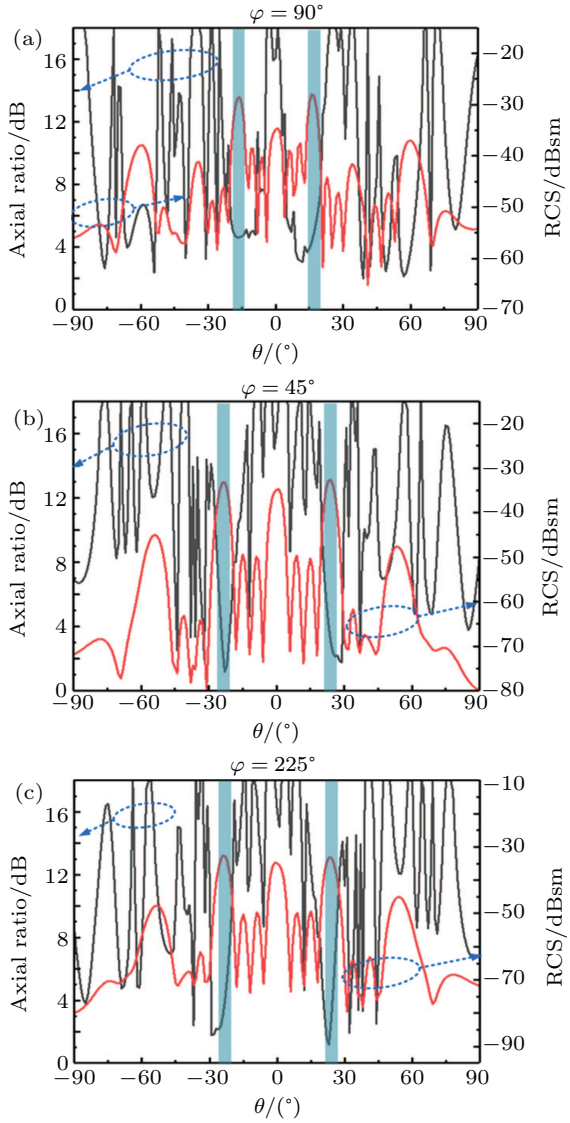



**Fig. 8.** Axial ratio and RCS of the reflected wave in $\varphi = 90°$ (a), $\varphi = 45°$ (b), and $\varphi = 225°$ (c) with $S_1$ coding metasurface under normal incidence of LP wave at 1.85 THz.

## 4. Conclusion

To sum up, a novel coding metasurface has been proposed to achieve high-efficiency polarization conversion in the terahertz region. It can simultaneously realize the linear-to-circular polarization conversion and cross polarization conversion. The axial ratio shows that polarization conversion is high-efficiency by using the proposed coding metasurface, which is less than 3 dB at 1.85 THz. The theoretical predictions are agreement well with the simulated results. Due to its excellent polarization conversion performance of the proposed coding metasurface, it can be used for terahertz polarization convertor and unidirectional transmission devices.

## References

[1] Yu N, Genevet P, Kats M A, Aieta F, Tetienne J P, Capasso F and Gaburro Z 2011 *Science* **334** 333
[2] Pendry J B, Schurig D and Smith D R 2006 *Science* **312** 1780
[3] Smith D R, Padilla W J, Vier D, Nemat-Nasser S and Schultz S 2000 *Phys. Rev.* **84** 4184
[4] Sui S, Ma H, Wang J F, Pang Y Q, Feng M D, Xu Z and Qu S B 2017 *J. Phys. D: Appl. Phys.* **51** 065603
[5] Li Y F, Zhang J M, Qu S B, Wang J F, Chen H Y, Xu Z and Zhang A X 2014 *Appl. Phys. Lett.* **104** 221110
[6] Wen D D, Yue F Y, Li G X, Zheng G X, Chan K L, Chen S M, Chen M, Li K F, Wong P W H, Cheah K W, Pun E Y B, Zhang S and Chen X Z 2015 *Nat. Commun.* **6** 8241
[7] Sun G, Chen H, Cheng S and Zhao X 2017 *Physica B* **525** 127
[8] Xu H, Tang S, Ling X, Luo W and Zhou L 2017 *Ann. Physik* **529** 1700045
[9] Sui S, Ma H, Wang J F, Feng M D, Pang Y Q, Xia S, Xu Z and Qu S B 2016 *Appl. Phys. Lett.* **109** 014104
[10] Sun H Y, Gu C Q, Chen X L, Li Z, Liu L L and Martin F 2017 *J. Appl. Phys.* **121** 174902
[11] Gao X, Han X, Cao W P, Li H O, Ma H F and Cui T J 2015 *IEEE Trans. Antenn Propag.* **63** 3522
[12] Liu C B, Bai Y, Zhao Q, Yang Y H, Chen H S, Zhou J and Qiao L J 2016 *Sci. Rep.* **6** 34819
[13] Liu S, Cui T J, Xu Q, Bao D, Du L L, Wan X, Tang W X, OuYang C M, Zhou X Y, Yuan H, Ma H F, Jiang W X, Han J G, Zhang W L and Chen Q 2016 *Light Sci. Appl.* **5** e16076
[14] Zhuang Y Q, Wang G M, Cai T and Zhang Q F 2018 *Opt. Express* **26** 3594
[15] Zhu H and Semperlotti F 2016 *Phys. Rev. Lett.* **117** 034302
[16] Jing Y, Li Y F, Zhang J F, Wang J, Feng M C, Ma H and Qu S B 2019 *Opt. Express* **27** 21520
[17] Jing Y, Li Y, Zhang J M, Wang J, Feng M, Sui S, Qiu T, Ma H and Qu S 2018 *J. Phys. D: Appl. Phys.* **51** 475103
[18] Cui T J, Qi M Q, Wan X, Zhao J and Cheng Q 2014 *Light Sci. Appl.* **3** e218